Geotechnical, Geological and Earthquake Engineering 33

Gian Paolo Cimellaro · Satish Nagarajaiah · Sashi K. Kunnath *Editors*

Computational Methods, Seismic Protection, Hybrid Testing and Resilience in Earthquake Engineering

A Tribute to the Research Contribution of Prof. Andrei Reinhorn

The book is a tribute to the research contribution of Professor Andrei Reinhorn in the field of earthquake engineering. It covers all the aspects connected to earthquake engineering starting from computational methods, hybrid testing and control, resilience and seismic protection which have been the main research topics in the field of earthquake engineering in the last 30 years. These were all investigated by Prof. Reinhorn throughout his career. The book provides the most recent advancements in these four different fields, including contributions coming from six different countries giving an international outlook to the topics.

Earth Sciences

ISBN 978-3-319-06393-5

9 783319 063935

▶ springer.com

GGEE 33 Cimellaro · Nagarajaiah Kunnath *Eds.*

Computational Methods, Seismic Protection, Hybrid Testing and Resilience in Earthquake Engineering

Geotechnical, Geological and Earthquake Engineering

Gian Paolo Cimellaro
Satish Nagarajaiah
Sashi K. Kunnath *Editors*

Computational Methods, Seismic Protection, Hybrid Testing and Resilience in Earthquake Engineering

A Tribute to the Research Contribution of Prof. Andrei Reinhorn

Springer

3D BASIS Origins, Novel Developments and Its Impact in Real Projects around the World

Satish Nagarajaiah [1]

[1] Professor, Civil & Env. Engineering and Mech. Engineering
Rice University, Houston, Texas, USA
[1]e-mail: Satish.Nagarajaiah@rice.edu

Abstract Origins and development of **3D-BASIS** (**3-D**imensional **BAS**e **I**solated **S**tructures) was initially envisioned by the need for an efficient tool for nonlinear dynamic analysis of three-dimensional base isolated structures, particularly in solving the highly nonlinear bidirectional stick-slip hysteretic response of a collection of sliding isolation bearings and the resulting response of the superstructure, as this was not available at that time. The primary challenge was to solve the stick-slip behavior of friction bearings—modeled using a differential equation (Bouc-Wen Model) due to its efficiency in representing constant Coulomb friction or variable velocity depended friction by using a very small yield displacement during the stick phase resulting in very high tangential stiffness followed by a very small tangential stiffness during the sliding phase—and the resulting stiff differential equations. A challenge that is compounded when biaxial-friction is modeled, wherein even the traditional method of using Gear's method to solve stiff differential equations breaks down—a problem that was vexing the research team at University at Buffalo trying to solve the problem at that time. The answer was the development of the novel pseudo-force solution algorithm along with a semi-implicit Runge-Kutta method to solve the difficult problem. The efficient solution procedure is needed primarily for the nonlinear isolation system consisting of (1) sliding and/or elastomeric bearings, (2) fluid dampers, (3) other energy dissipation devices, while the superstructure is represented by three dimensional superstructure model appropriately condensed (where only master nodes at the center of mass of the floor are retained). This chapter describes the origins, development of 3D-BASIS and its impact.

1 Introduction

Base isolation involves the introduction of isolation bearings and energy dissipating devices between the superstructure and its foundation. The laterally flexible isolation system shifts the fundamental period—considering an equivalent linear isolation system—of the structure beyond its fixed base period and the predominant periods of the ground motion. The period lengthening to typically 2

to 4 sec is sufficient to reflect the earthquake energy. Energy dissipation in the isolation system is then useful in limiting the displacement response. The isolation bearings generally exhibit material nonlinearities and under certain conditions may also exhibit geometric nonlinearities. However, these nonlinearities are restricted to the isolation system. The superstructure is typically designed to exhibit elastic behavior.

This chapter presents a brief overview of the analytical modeling techniques used in the nonlinear dynamic analysis of base isolated structures. The localized nonlinearities at the base allow condensation of the linear superstructure to a small number of master degrees of freedom. All the nonlinear bearings and devices are explicitly modeled.

Mechanical properties of isolation bearings are described in detail. Material, friction, geometric and contact nonlinearities in the isolation system are discussed. Analytical models used for characterizing the behavior of isolation bearings and devices are presented. Formulation of the combined linear superstructure and nonlinear isolation system and solution procedure is presented. Computer programs that are most popularly used are described briefly.

2 Base isolation systems

Base isolation systems have gained wide acceptance [1-4]. The isolation bearings are typically connected between columns and foundation as shown in Figure 1. The isolation system is designed to be very stiff in the vertical direction. The isolation system is designed to provide adequate initial stiffness under service loads, such as wind load, and to provide greater flexibility past yielding of the isolation bearings under strong ground motion or seismic loads.

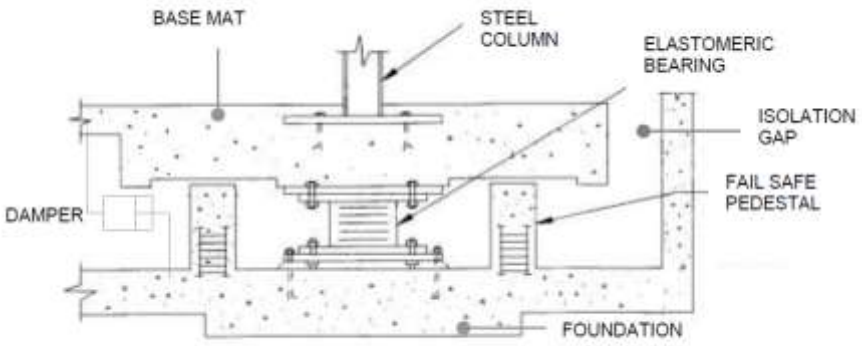

Fig. 1 – Isolation System Details Including Elastomeric Bearing and Damper

There are two basic types of isolation bearings: elastomeric bearings and sliding bearings. Elastomeric bearings consist of laminated rubber layers and steel shim plates. Two types of elastomeric bearings that have been implemented in structures are the high damping rubber bearing and the lead rubber bearing. In both types the laminated rubber provides the lateral flexibility. The isolation system level displacements increase due to the lateral flexibility. Adding energy dissipation capacity reduces the isolation system displacements. The energy dissipation capacity is provided by the inherent damping capacity of the rubber in high damping bearings. In lead-rubber bearings, which are typically manufactured with low damping rubber, the cylindrical lead plug within the rubber unit provides the energy dissipation capacity. Moreover, supplemental energy dissipating devices, primarily in the form of fluid viscous dampers, have been used in isolation systems to substantially enhance damping in applications in areas of very high seismicity.

Sliding bearings consist of Teflon or similar materials sliding on a stainless steel surface. Two types of sliding bearings that have been implemented in structures are the Friction Pendulum Sliding (FPS) bearings, spherically shaped sliding bearings, and the flat sliding bearings. Sliding bearings dissipate energy due to friction. Restoring force is provided by the spherical sliding surface in the FPS system or by added springs in the system with flat sliding bearings.

3 Material/Friction nonlinearities of base isolation bearings and devices

3.1 Elastomeric Bearings

Elastomeric bearings are typically made of natural rubber and are classified into low damping and high damping bearings. The low damping bearings exhibit shear stiffness which is effectively linear to large shear strains (>100%). The damping is in the range of 2 to 5 % of critical. Lead-rubber bearings are made up of low damping natural rubber with a lead core. The lead core is provided to increase the energy dissipation capacity to about 20 to 30% of critical. The idealized force displacement behavior of a lead-rubber bearing can be characterized as bilinear hysteretic as shown in Figure 2. The high initial stiffness offers rigidity under wind load and low level seismic load. The characteristic strength, $Q = A_p \sigma_{YL}$, where A_p is the lead plug area and σ_{YL} is the effective shear yield stress of lead. The post yielding stiffness, K_p, is typically higher than the shear stiffness of the bearing without the lead core

$$K_p = \frac{A_r G}{\sum t} f \tag{1}$$

Where, A_r is the bonded rubber area, $\sum t$ is the total rubber thickness, G is the shear modulus of rubber, and f is a factor larger than unity. Under proper conditions, f, may be equal to or less than 1.15. Moreover, the initial elastic stiffness, K_e, ranges between 6.5 to 10 times the post-yielding stiffness.

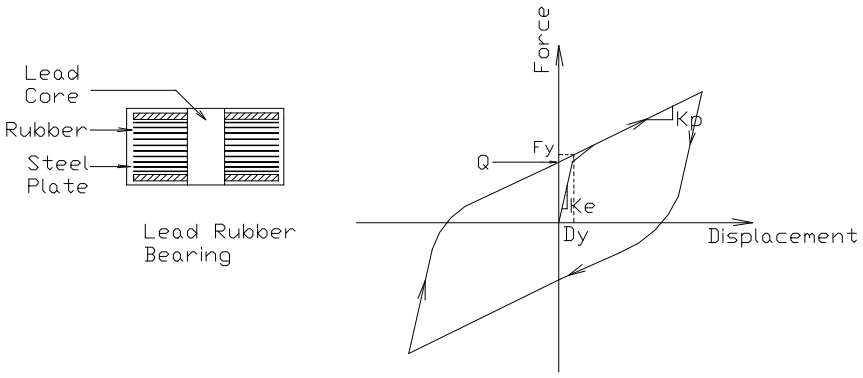

Fig. 2 – Lead Rubber Bearing: Bilinear Force-Displacement Loop

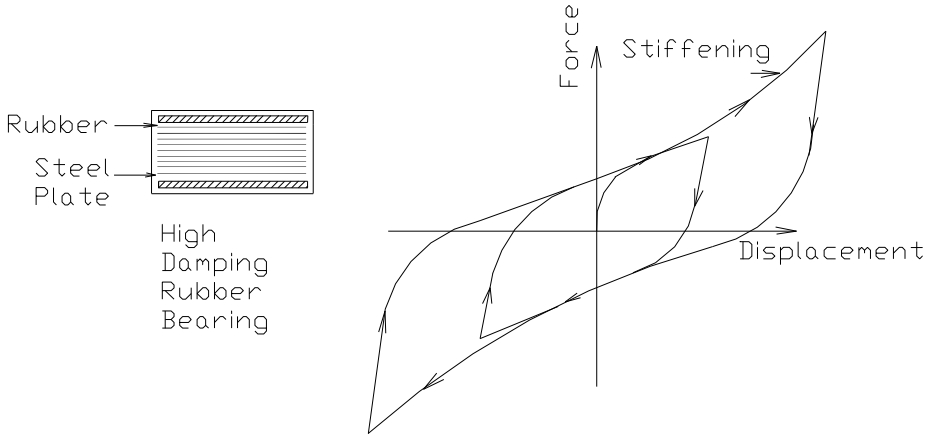

Fig. 3 – High Damping Bearing: Force Displacement Loop with Stiffening

The stiffness and energy dissipation characteristics of high damping bearings are highly nonlinear and dependent on shear strain as shown in Figure 3. The high

damping bearings are made up of specially compounded rubber, which provides effective damping of 10 to 15 % of critical. The high damping bearings have high shear stiffness at low shear strains (< 20%) for rigidity under wind load and low level seismic load. The shear stiffness is typically lower in the range of 20 to 120 % shear strains. At large shear strains, the shear stiffness increases due to strain crystallization process in the rubber. The damping in high damping bearings is best characterized by a combination of hysteretic and viscous behavior. In the virgin stage and during the first cycle of movement, the bearings exhibit higher stiffness and damping than in the following cycles. The stiffness stabilizes by the third cycle, resulting in stable properties termed as scragged properties. Scragging of the bearings is the result of internal changes in the rubber. Recovery to the unscragged (virgin) properties occurs following sufficient time. The scragged state of the bearings can be modeled by a bilinear hysteretic model for shear strains of up to 200%. The stiffening behavior (see Figure 3) beyond this strain can also be modeled using more complex models [5-7]. The current technique used to model high damping bearings is to perform multiple analysis with bilinear hysteretic models; the parameters of the bilinear hysteretic models are determined at specific shear strain amplitudes. The bilinear model parameters can be established from test data of prototype bearings. These properties are the shear modulus, G, and the equivalent damping ratio, ξ (defined as the energy dissipated in a cycle of motion divided by 4π and by the maximum kinetic energy) under scragged conditions. G, is related to the post yielding stiffness K'_p

$$K'_p = \frac{GA_r}{\sum t} \tag{2}$$

The parameters of the model may be determined by use of the mechanical properties of *G* and ξ at a specific strain- for example parameters corresponding to the design displacement. The post yielding stiffness, K'_p, is determined from (2), where as the characteristic strength, Q, may be related to the mechanical properties by assuming bilinear hysteretic behavior

$$Q = \frac{\pi \xi K'_p D^2}{(2 - \pi \xi)D - 2Dy} \tag{3}$$

Where, the yield displacement, *Dy*, is between 0.05 and 0.1 times the total rubber thickness and *D* is the design displacement. The yield force, *Fy*, is given by

$$Fy = Q + K'_p Dy \tag{4}$$

and the post to pre-yielding stiffness ratio is given by

$$\alpha = \frac{K'_p Dy}{Fy} \tag{5}$$

Elastomeric bearings have finite vertical stiffness that affects the vertical response of the isolated structure. The vertical stiffness of an elastomeric bearing can be estimated as follows

$$k_v = \frac{E_c A_r}{\sum t} \tag{6}$$

Where, E_c is the compression modulus.

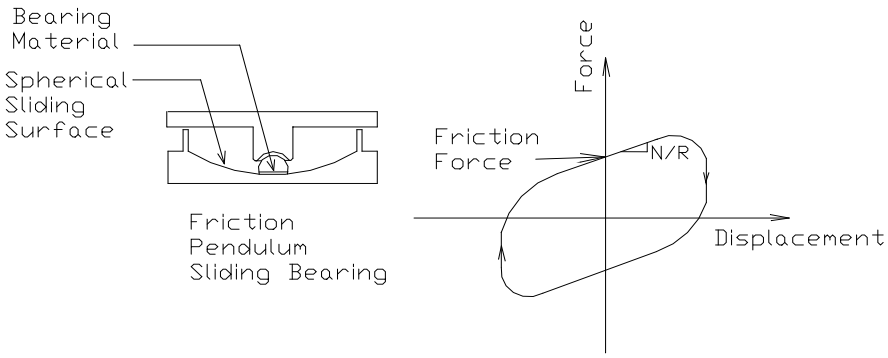

Fig. 4 – Friction Pendulum Bearing: Force-Displacement Loop (includes Friction and Recentering Force)

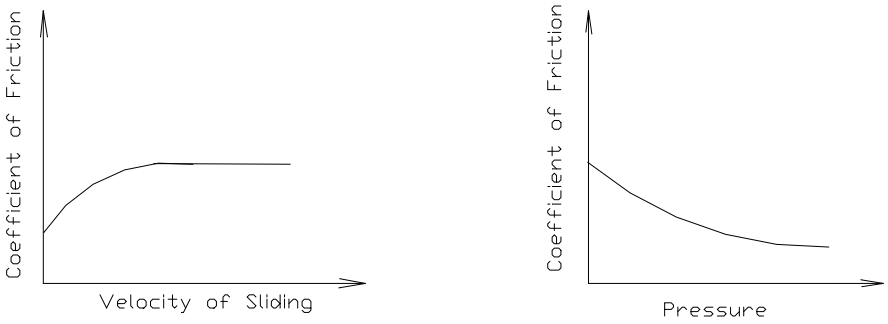

Fig. 5 – Variation of Coefficient of Friction as a function of velocity of sliding and pressure

3.2 Sliding Bearings

Two types of sliding bearings are the flat sliding bearings with restoring force devices and the friction pendulum bearings (FPS) shown in Figure 4. Flat sliding bearing is made up of Teflon sliding on a flat stainless steel surface. The recentering capability is provided by additional elastic springs. The FPS bearing, shown in Figure 4, is made up of a composite material sliding on a spherical surface with radius of curvature R, which provides the recentering force. The behavior of FPS bearing can be represented by

$$F = \frac{N}{R}U + \mu_s N \operatorname{sgn}(\dot{U}) \tag{7}$$

Where, F is the force in the bearing, U and $\dot{U}$ are the displacement and velocity, respectively, μ_s is the coefficient of sliding friction (dependent on velocity and pressure) and N is the normal load on the bearing. It should be noted that for flat sliding bearings R is infinite. The coefficient of friction of sliding bearings depends on a number of parameters of which the composition of the sliding interface, bearing pressure and velocity of sliding (as shown in Figure 5) are the most important. For interfaces consisting of polished stainless steel in contact with Teflon or composites the coefficient of friction may be described by [8]

$$\mu_s = f_{\max} - (f_{\max} - f_{\min}) \exp\left(-a\left|\dot{U}\right|\right) \tag{8}$$

Where the parameters $f_{\min}$ and $f_{\max}$ describe, respectively, the coefficients of friction at essentially zero and large velocities of sliding and under constant pressure. Parameters $f_{\min}$, $f_{\max}$ and a depend on the bearing pressure, although only the dependency of $f_{\max}$ on pressure is of practical significance.

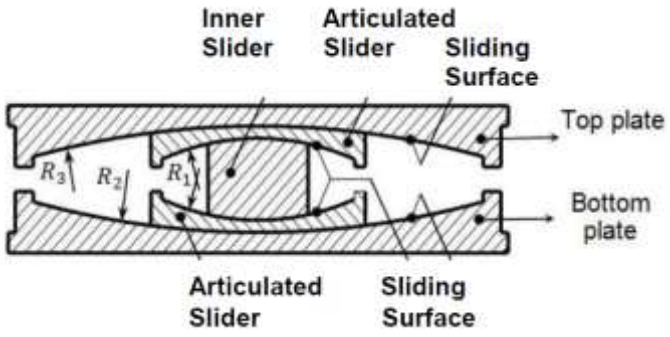

Fig. 6 – Triple Friction Pendulum Isolator

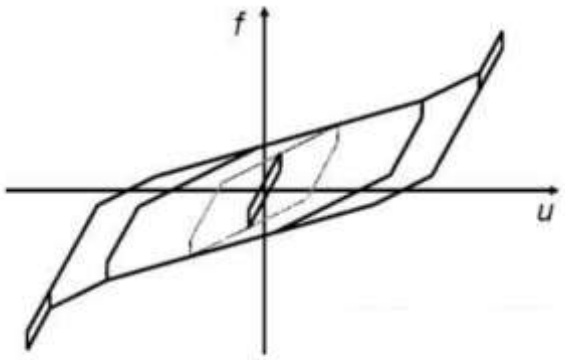

Fig. 7 – Force (f) - Displacement (u) Behavior of Triple Friction Pendulum Isolator

More recently Fenz and Constantinou [9,10], Morgan and Mahin [11], Ray and Reinhorn [12] and Dao et al. [13] have studied the triple friction pendulum isolation bearing that has an inner slider and articulated sliders sliding inside concave sliding surfaces as shown in Figure 6, and developed detailed analytical models with force-displacement behavior as shown in Figure 7.

3.3 Fluid Viscous Dampers

Fluid dampers [14] are used to enhance the damping in the isolation system and are connected between the base and foundation as shown in Figure 1. Fluid viscous dampers produce force by forcing fluid (typically silicone oil) through orifice passages as shown in Figure 8. It is possible to shape the orifice passages [14] in such a way as to produce an output force of the type

$$F = C \left| \dot{U} \right|^{\alpha} \operatorname{sgn}(\dot{U}) \tag{9}$$

Where C = damping coefficient, α is in the range of 0.5 to 1.0 and the representative force-displacement loops are shown in Figure 8.

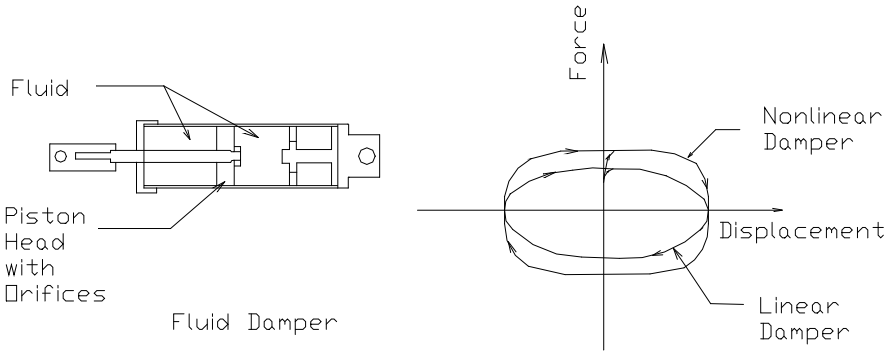

Fig. 8 – Fluid Damper: Force Displacement Loop (Velocity Dependent Damping Force)

4 Modeling material/friction nonlinearities of isolation bearings

Models with bilinear hysteretic characteristics can represent the behavior of elastomeric bearings. Several models have been used to represent the uniaxial and biaxial behavior of elastomeric isolation bearings. The uniaxial and biaxial behavior of elastomeric bearings have been modeled by Nagarajaiah [15], Nagarajaiah et al. [16,17] using a viscoplasticity based modified Bouc-Wen model [18-20]. In the biaxial model forces F_X and F_Y are mobilized during the motion along the X and Y directions, respectively, of the elastomeric bearing:

$$F_X = \alpha \frac{Fy}{Dy} U_x + (1-\alpha) FyZ_x \qquad F_Y = \alpha \frac{Fy}{Dy} U_y + (1-\alpha) FyZ_y \quad (10)$$

in which α is the post-yielding to pre-yielding stiffness ratio, Fy is the yield force and Dy is the yield displacement. Z_x and Z_y are dimensionless variables governed by the following differential equations, which were proposed by [20]

$$\begin{aligned} Dy\dot{Z}_x + \gamma \left|\dot{U}_x Z_x\right| Z_x + \beta \dot{U}_x Z_x^2 + \gamma \left|\dot{U}_y Z_y\right| Z_x + \beta \dot{U}_y Z_x Z_y - A\dot{U}_x = 0 \\ Dy\dot{Z}_y + \gamma \left|\dot{U}_y Z_y\right| Z_y + \beta \dot{U}_y Z_y^2 + \gamma \left|\dot{U}_x Z_x\right| Z_y + \beta \dot{U}_x Z_y Z_x - A\dot{U}_y = 0 \end{aligned} \quad (11)$$

Parameters A, β and γ are dimensionless—$A/(\beta+\gamma)$=1 is chosen—and U_x, U_y and $\dot{U}_x, \dot{U}_y$ represent, respectively, the displacements and velocities that occur

at the isolation bearing. It can also be shown that the interaction curve of this biaxial model is circular.

In sliding bearings Teflon undergoes a small elastic shear deformation (less than 2 mm) before sliding commences. The small shear deformation of Teflon renders a finite but high elastic stiffness to the hysteretic loop, which can be captured by a hysteretic model. A hysteretic model for sliding bearings, which can account for the variation of coefficient of friction with velocity and bearing pressure observed in Teflon sliding bearings, has been presented by [6,8,16,21].

FPS bearings have been modeled using the hysteretic model in (11) with yield displacement, *Dy,* being very small (typically less than 2 mm)

$$F_X = \frac{N}{R}U_x + \mu_s NZ_x, \qquad F_Y = \frac{N}{R}U_y + \mu_s NZ_y \tag{12}$$

Where, μ_s is the coefficient of sliding friction and N is the normal load on the bearing. The normal load consists of gravity load, W, the effect of vertical ground acceleration, $\ddot{U}_v$, and the additional seismic load, P_{sl}, due to overturning moment

$$N = W\left(1 + \frac{\ddot{U}_v}{g} + \frac{P_{sl}}{W}\right) \tag{13}$$

Where, g is the acceleration due to gravity. It should be noted that for flat sliding bearings R is infinite and (12) collapses to the model described in Constantinou et al. [8] and Nagarajaiah et al. [16] and experimentally verified by Mokha et al. [21]. A representative biaxial force-displacement behavior of flat slider is shown in Figure 9. The eight shaped biaxial behavior is observed to have significant effect on the force-displacement behavior in the X direction.

Plasticity based models have been used to model isolation elements [22]. Modified rate models have been used to represent the behavior of high damping bearings including stiffening [6,7].

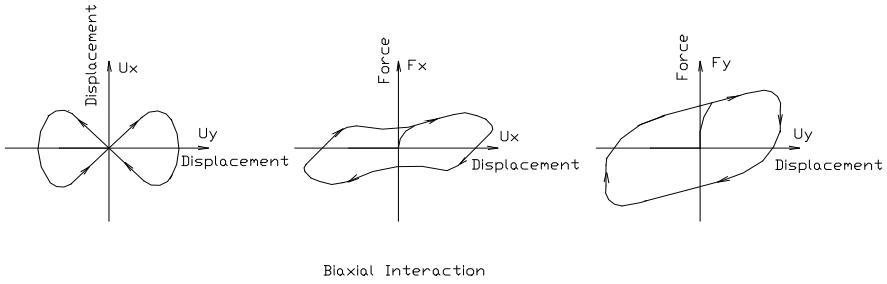

Fig. 9 – Biaxial Force-Displacement Behavior of Flat Sliding Bearing: (a) Biaxial Displacement Profile, (b) Force-Displacement Response – X Direction; (c) Force-Displacement Response – X Direction

5 Geometric nonlinearities of base isolation bearings

5.1 Axial Load – Horizontal Displacement Effects

The elastomeric bearings when subjected to large axial forces and lateral horizontal displacements exhibit nonlinear and unstable behavior. This behavior is due to a combination of both geometric and material nonlinearities. The shear-force and horizontal displacement, *F-u,* curves are shown in Figures 10 and 11.

The connection of elastomeric bearings can be either doweled or bolted to the column above and foundation below, which influences the behavior of the bearing. In doweled bearings rollover occurs and the displacement at which it commences can be calculated [23]. The rollover behavior can be modeled by including the P-Δ effects. In addition, since the bearing cannot sustain upward axial force because of doweled connection, uplift needs to be considered (as shown in Figure 11).

Sliding bearings are stable even under large displacements. The change is axial load effects the coefficient of friction. Tsopelas et al. [6] and Nagarajaiah [24] have modeled the influence of axial load on the coefficient of friction.

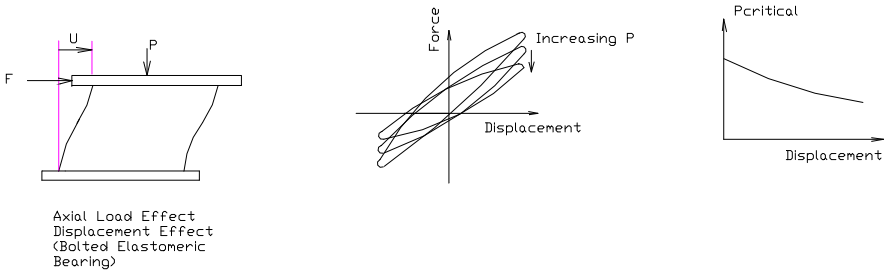

Fig. 10 – Large Axial Load-Horizontal Displacement Behavior of Elastomeric Bearings: (a) Bearing; (b) Horizontal Force-Displacement Behavior; (c) Critical Load as a Function of Horizontal Displacement

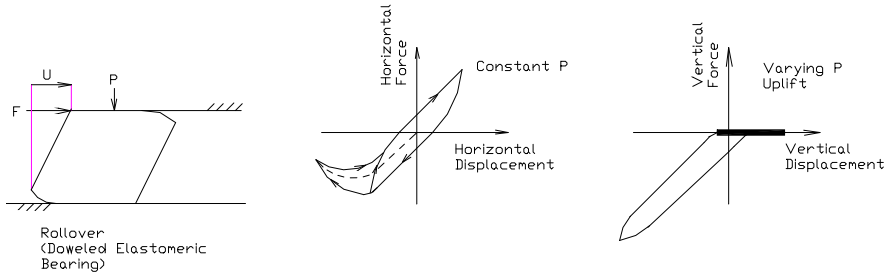

Fig. 11 – Large Axial Load-Horizontal Displacement Behavior of Elastomeric Bearings with Rollover: (a) Bearing with Rollover; (b) Horizontal Force- Displacement Behavior with Rollover; (c) Vertical Force–Vertical Displacement Behavior

6 Modeling geometric nonlinearities of isolation bearings

The axial load effect on elastomeric bearings has been modeled using linear models [25]. A nonlinear analytical model has been developed by Nagarajaiah et al. [26], based on Koh-Kelly model, to include the effect of axial load and horizontal displacement. The large axial load horizontal behavior leads reduction in stiffness due to increasing axial load and reduction in critical axial load due to large horizontal displacement as shown in Figure 10.

The critical load and horizontal displacement, P_{cr}-u, curves using the nonlinear analytical model developed by Nagarajaiah et al. [26] are shown in Figure 10 (c) which demonstrates that the bearing critical load drops with increasing horizontal displacement. The equilibrium paths demonstrate unstable post-critical behavior as observed in the experimental results. The critical load occurs at the limit point of each equilibrium path and horizontal tangential stiffness is zero at the limit point. The critical load drops with increasing horizontal displacement because the equilibrium paths are unstable. More details can be found in Constantinou et al. [5].

7 Contact nonlinearities of base isolation systems

7.1 Uplift

Uplift occurs in doweled elastomeric bearings and in sliding bearings, due to loss of contact at the bearing as the column experiences axial tension forces (Figure 11(c)). This loss of contact is reestablished as the cycle of motion reverses with compression forces in the column. Uplift is generally beneficial and reduces the base shear forces further [24]. The effect of uplift can be modeled using a contact element with only compression stiffness ([24,27-29], SAP [22]).

7.2 Pounding

The isolation gap (see Figure 1) around the base isolated structure is provided to permit the maximum design displacement. Long period motions, as observed in 1994 Northridge earthquake and other recent earthquakes, could cause large base displacements. In such cases, unless appropriate measures are taken, pounding can occur accompanied by varying degree of damage to the superstructure. In the measured response of base isolated structures, subjected to Northridge earthquake, pounding has been observed when the isolation gap was not fully functional. The effect of pounding can be modeled by using gap elements [30].

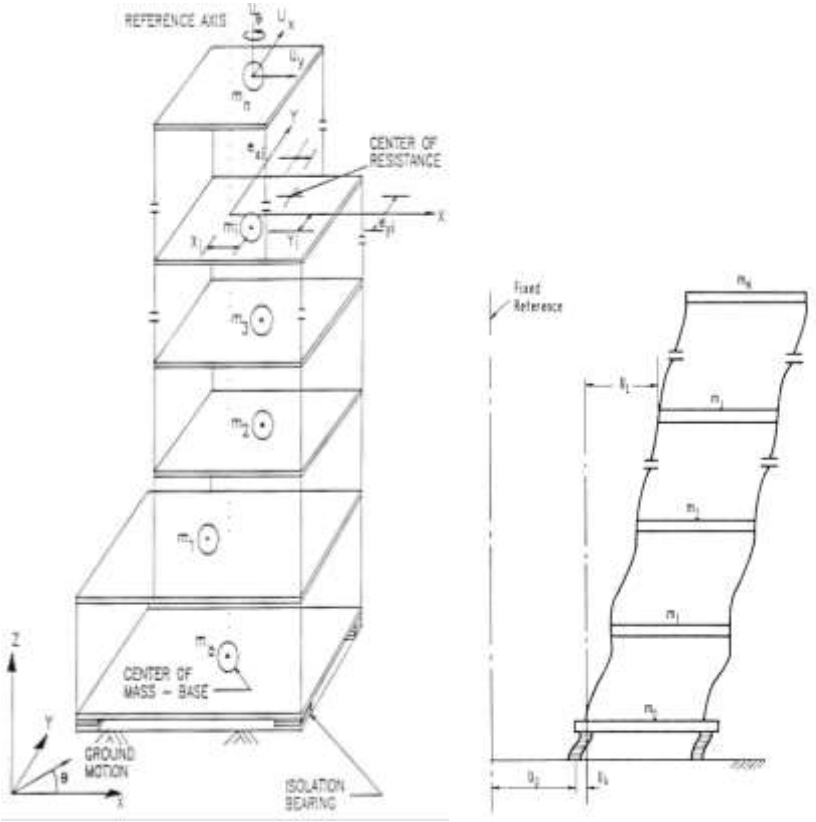

Fig. 12 – (a) Asymmetric Base Isolated Structure Excited by Bidirectional Ground Motion, (b) Displacement Coordinates

8 Superstructure and isolation system modeling and solution procedures

The formulation and pseudoforce solution algorithm developed by Nagarajaiah [15], Nagarajaiah et al. [16,17], which has been implemented in widely used computer program 3D-BASIS [16] for analyzing base isolated structures, is presented next. This is followed by brief description of the Ritz vector formulation and solution algorithm developed by Wilson [28] for the widely used computer programs SAP-ETABS [22].

8.1 Linear Superstructure and Nonlinear Isolation System

The superstructure, shown in Figure 12, is treated as a linear elastic system. The superstructure and the base are modeled with three degrees of freedom per floor at the center of mass as shown in Figure 12(a). The base and floors are assumed to be infinitely rigid in plane. The isolation system consisting of elastomeric or friction isolation bearings is modeled using discrete nonlinear biaxial elements. The equations of motion for the elastic superstructure are expressed in the following form

$$M\ddot{u} + C\dot{u} + Ku = -M\ R(\ddot{u}_g + \ddot{u}_b) \tag{14}$$

Where, M , C , K are the superstructure mass, damping, and stiffness matrices in the fixed base condition, and R is the influence matrix. Furthermore, $\ddot{u}, \dot{u},$ and u represent the floor acceleration, velocity, and displacement vectors relative to the base, $\ddot{u}_b$ the vector of base acceleration relative to the ground, and $\ddot{u}_g$ the vector of ground acceleration (see Figure 12(b)).

The equations of motion for the base are as follows

$$R^T M[\ddot{u} + R(\ddot{u}_b + \ddot{u}_g)] + M_b(\ddot{u}_b + \ddot{u}_g) + C_b\dot{u}_b + K_b u_b + f = 0 \tag{15}$$

Where, M_b = the diagonal mass matrix of the rigid base, C_b = the resultant damping matrix of viscous isolation elements, K_b = the resultant stiffness matrix of elastic isolation elements, and f = the global vector containing the forces mobilized in the nonlinear isolation elements with appropriate transformations. Employing modal reduction

$$u = \varphi\, u^* \tag{16}$$

Where, ϕ = the modal matrix, normalized with respect to the mass matrix, u^* = the modal displacement vector relative to the base. Combining eqns. (14) to (16), the following matrix equation is obtained

$$\begin{bmatrix} \varphi^T M\varphi & \varphi^T MR \\ R^T M\varphi & R^T MR + M_b \end{bmatrix} \begin{Bmatrix} \ddot{u}^* \\ \ddot{u}_b \end{Bmatrix} + \begin{bmatrix} \varphi^T C\varphi & O \\ O & C_b \end{bmatrix} \begin{Bmatrix} \dot{u}^* \\ \dot{u}_b \end{Bmatrix} + \begin{bmatrix} \varphi^T K\varphi & O \\ O & K_b \end{bmatrix} \begin{Bmatrix} u^* \\ u_b \end{Bmatrix} + \begin{Bmatrix} O \\ f \end{Bmatrix}$$
$$= -\begin{bmatrix} \varphi^T MR \\ R^T MR + M_b \end{bmatrix} \ddot{u}_g \qquad (17)$$

Since the modal matrix ϕ is normalized with respect to mass, the following diagonal matrices are obtained $\varphi^T M\varphi = I$, $\varphi^T K\varphi = \omega^2$ and $\varphi^T C\varphi = 2\zeta\omega$, where ω = diagonal matrix of natural frequencies of the fixed base structure, ζ = diagonal matrix of damping ratios of the fixed base structure. The formulation in (17) developed by [15] facilitates efficient solution using pseudoforce algorithm.

8.2 Pseudoforce Formulation and Solution Algorithm

Eqn. (17) can be written as follows:

$$\tilde{M}\ddot{\tilde{u}}_t + \tilde{C}\dot{\tilde{u}}_t + \tilde{K}\tilde{u}_t + f_t = \tilde{P}_t \qquad (18)$$

At time t+ Δ t

$$\tilde{M}\ddot{\tilde{u}}_{t+\Delta t} + \tilde{C}\dot{\tilde{u}}_{t+\Delta t} + \tilde{K}\tilde{u}_{t+\Delta t} + f_{t+\Delta t} = \tilde{P}_{t+\Delta t} \qquad (19)$$

Written in incremental form

$$\tilde{M}\Delta\ddot{\tilde{u}}_{t+\Delta t} + \tilde{C}\Delta\dot{\tilde{u}}_{t+\Delta t} + \tilde{K}\Delta\tilde{u}_{t+\Delta t} + \Delta f_{t+\Delta t} = \tilde{P}_{t+\Delta t} - \tilde{M}\ddot{\tilde{u}}_t - \tilde{C}\dot{\tilde{u}}_t - \tilde{K}\tilde{u}_t - f_t \qquad (20)$$

Where $\tilde{M}, \tilde{C}, \tilde{K}$,and $\tilde{P}$ represent the reduced mass, damping, stiffness, and load matrices in (20). Furthermore, the state of motion of modal superstructure and base is represented by vectors $\ddot{\tilde{u}}_t, \dot{\tilde{u}}_t, \tilde{u}_t$ in (17).

The incremental nonlinear global force vector $\Delta f_{t+\Delta t}$ in (20) is unknown. This global vector is brought on to the right hand side of (20) and treated as a pseudoforce vector. The two-stage solution algorithm developed by [15] involves the following steps: the solution of equations of motion using the unconditionally stable Newmark's constant average acceleration method, in the first stage and the solution of differential equations governing the behavior of the nonlinear isolation elements using the unconditionally stable semi-implicit Runge-Kutta method [31], suitable for solutions of stiff differential equations, in the second stage. Furthermore, an iterative procedure consisting of corrective pseudoforces is employed within each time step until global equilibrium is achieved. The pseudoforce method with iteration is efficient due to the coefficient matrix of the

equation of motion is formed and factorized only once at the beginning of the solution and repeatedly used. The method is particularly efficient due to the localized nonlinearities in the isolation elements that exist only at the base of the structure. The pseudoforce method converges to the correct solution even when severe nonlinearities such as planar sliding behavior along with biaxial effects are present. The method yields results of comparable accuracy of the predictor-corrector method [15].

The developed solution algorithm is as follows:

1. Initial Conditions.

a. Form stiffness matrix $\tilde{K}$, mass matrix $\tilde{M}$, and damping matrix $\tilde{C}$. Initialize $\tilde{u}_o, \dot{\tilde{u}}_o$ and $\ddot{\tilde{u}}_o$.

b. Select time step Δt, set parameters $\delta = 0.25$ and $\theta = 0.5$, and calculate the integration constants:

$$a_1 = \frac{1}{\delta(\Delta t)^2}, \quad a_2 = \frac{1}{\delta \Delta t}, \quad a_3 = \frac{1}{2\delta}$$

$$a_4 = \frac{\theta}{\delta \Delta t}, \quad a_5 = \frac{\theta}{\delta}, \quad a_6 = \Delta t\left(\frac{\theta}{2\delta} - 1\right)$$

c. Form the effective stiffness matrix

$$K^* = a_1\tilde{M} + a_4\tilde{C} + \tilde{K} \tag{21}$$

d. Triangularize K^* using Gaussian elimination (only if the time step is different from the previous step).

2. Iteration at each time step.

a. Assume the global pseudoforce vector

$$\Delta f^i_{t+\Delta t} = 0$$

in iteration i =1.

b. Calculate the effective load vector at time $t + \Delta t$:

$$P^*_{t+\Delta t} = \Delta\tilde{P}_{t+\Delta t} - \Delta f^i_{t+\Delta t} + \tilde{M}\left(a_2\dot{\tilde{u}}_t + a_3\ddot{\tilde{u}}_t\right) + \tilde{c}\left(a_5\dot{\tilde{u}}_t + a_6\ddot{\tilde{u}}_t\right) \tag{22}$$

$$\Delta\tilde{P}_{t+\Delta t} = \tilde{P}_{t+\Delta t} - \left(\tilde{M}\ddot{\tilde{u}}_t + \tilde{C}\dot{\tilde{u}}_t + \tilde{K}\tilde{u}_t + f_t\right) \tag{23}$$

c. Solve for displacements at time $t + \Delta t$:

$$K^*\Delta u^i_{t+\Delta t} = P^*_{t+\Delta t} \tag{24}$$

d. Update the state of motion at time $t + \Delta t$:

$$\begin{aligned}\ddot{\tilde{u}}_{t+\Delta t} &= \ddot{\tilde{u}}_t + a_1 \Delta\tilde{u}^i_{t+\Delta t} - a_2\dot{\tilde{u}}_t - a_3\ddot{\tilde{u}}_t \\ \dot{\tilde{u}}_{t+\Delta t} &= \dot{\tilde{u}}_t + a_4 \Delta\tilde{u}^i_{t+\Delta t} - a_5\dot{\tilde{u}}_t - a_6\ddot{\tilde{u}}_t \\ \tilde{u}_{t+\Delta t} &= \tilde{u}_t + \Delta\tilde{u}^i_{t+\Delta t}\end{aligned} \tag{25}$$

e. Compute the state motion at each bearing and solve for the nonlinear forces at each bearing using the semi-implicit Runge-Kutta method.

f. Compute the nonlinear global force vector at the center of mass of the base $\Delta f^{i+1}_{t+\Delta t}$.

g. Compute

$$error = \frac{\left|\Delta f^{i+1}_{t+\Delta t} - \Delta f^{i}_{t+\Delta t}\right|}{ref.\max f} \tag{26}$$

Where, $|\bullet|$ is the Euclidean norm.

h. If error $\geq$ tolerance, further iteration is needed; iterate starting from step 2a and use $\Delta f^{i+1}_{t+\Delta t}$ as the pseudoforce vector and the state of motion at time t, $\tilde{u}_t, \dot{\tilde{u}}_t$ and $\ddot{\tilde{u}}_t$.

If error $\leq$ tolerance, no further iteration is needed; update the nonlinear global force vector $f_{t+\Delta t} = f_t + \Delta f^{i+1}_{t+\Delta t}$, reset time step if necessary, and go to step 2a if the time step is not reset or 1b if the time step is reset.

9 Semi-implicit Runge-Kutta procedure in 3D-BASIS

The semi-implicit Runge-Kutta procedure in 3D-BASIS [15, 16, 17] was developed by the author as a part of his Ph.D. dissertation [15], based on the original work of Rosenbrock [31]. The Bouc-Wen hysteretic model presented in equation (10) for uniaxial case (equation (11a-11b) for biaxial case) can be represented as follows:

$$\dot{z} = a_1 - a_2 z^{\eta} - a_3 z^{\eta} \tag{27}$$

The numerical procedure involves the following steps: Compute

$$z_{updated} = z_t + C_2 * k_r \tag{28}$$

Where,

$$k_r = \Delta t \left\{ \frac{1}{1 + \Delta t * C_1 * \left(-\frac{d\dot{z}_t}{dz} \right)} \right\} \dot{z}_t, \quad l_r = \Delta t \left\{ \frac{1}{1 + \Delta t * C_1 * \left(-\frac{d\dot{z}_t}{dz} \right)} \right\} \dot{z}_{updated}$$

Evaluate constants C_1 and C_2 using Rosenbrock's procedure [31] and Taylor series [see [15] for futher details]. Calculate constants. Formulate

$$\dot{z}_t = z_P(1,1) = A_1 - A_2 (z_t)^{\eta} - A_3 (z_t)^{\eta} \tag{29}$$

With

$$\begin{aligned} z_{updated} &= z_t + C_2 \times RK \\ \dot{z}_{updated} &= A_1 - A_2 \left(z_{updated} \right)^{\eta} - A_3 \left(z_{updated} \right)^{\eta} \end{aligned} \tag{30}$$

Where,

$$RK = \frac{\dot{z}_t \Delta t}{\left\{ 1 + C_1 \Delta t \left(-\frac{d\dot{z}_t}{dz} \right) \right\}}, \qquad -\frac{d\dot{z}_t}{dz} = \eta (z_t)^{\eta - 1} (A_2 + A_3)$$

Recalculate and then update

$$z_{t+\Delta t} = z_t + 0.75 \times RK + 0.25 \times RL \tag{31}$$

Where,

$$RL = \frac{\dot{z}_{updated} \Delta t}{\left\{ 1 + C_1 \Delta t \left(-\frac{d\dot{z}_t}{dz} \right) \right\}}, \qquad -\frac{d\dot{z}_t}{dz} = \eta (z_t)^{\eta - 1} (A_2 + A_3)$$

This innovative solution procedure has been used by many other researchers at University at Buffalo, since its development by the author [32].

In summary the algorithm is summarized in the following table.

A. Initial Conditions:

1. Form stiffness matrix $\mathbf{K}^*$, mass matrix $\mathbf{M}^*$, and damping matrix $\mathbf{C}^*$. Initialize $\mathbf{u}_0^*$, $\dot{\mathbf{u}}_0^*$ and $\ddot{\mathbf{u}}_0^*$

2. Select time step $\triangle t$, set parameters $\delta = 0.25$ and $\theta = 0.25$, and calculate the integration constants:

$$\alpha_1 = \frac{1}{\delta(\triangle t)^2}; \alpha_2 = \frac{1}{\delta(\triangle t)}; \alpha_3 = \frac{1}{\delta};$$
$$\alpha_4 = \frac{\theta}{\delta(\triangle t)^2}; \alpha_5 = \frac{\theta}{\delta(\triangle t)}; \alpha_6 = \frac{\theta}{\delta}$$

3. Form the effective stiffness matrix

$$\mathbf{K}' = \alpha_1 \mathbf{M}^* + \alpha_4 \mathbf{C}^* + \mathbf{K}^*$$

4. Triangularize $\mathbf{K}'$ using Gaussian elimination(only if the time step is different from the previous step).

B. Iteration at each time step:

1 Assume the pseudo-force $\triangle \mathbf{f}_{t+\triangle t}^i = 0$ in iteration $i = 1$.

2. Calculate the effective load vector at time $t + \triangle t$:

$$\mathbf{P}'_{t+\triangle t} = \triangle \mathbf{P}^*_{t+\triangle t} - \triangle \mathbf{f}^*_{t+\triangle t} + \mathbf{M}^*(\alpha_2 \dot{\mathbf{u}}_t^* + \alpha_3 \ddot{\mathbf{u}}_t^*) + \bar{\mathbf{C}}(\alpha_5 \dot{\mathbf{u}}_t^* + \alpha_6 \ddot{\mathbf{u}}_t^*),$$
$$\triangle \mathbf{P}^*_{t+\triangle t} = \mathbf{P}^*_{t+\triangle t} - (\mathbf{M}^* \ddot{\mathbf{u}}_t^* + \mathbf{C} \dot{\mathbf{u}}_t^* + \mathbf{K} \mathbf{u}_t^* + \mathbf{f}_t)$$

3. Solve for displacements at time $t + \triangle t$:

$$\mathbf{K}' \triangle \mathbf{u}^i_{t+\triangle t} = \mathbf{P}'_{t+\triangle t}$$

4. Update the state of motion at time $t + \triangle t$:

$$\ddot{\mathbf{u}}^*_{t+\triangle t} = \ddot{\mathbf{u}}^*_t + \alpha_1 \triangle \mathbf{u}^{*i}_{t+\triangle t} - \alpha_2 \dot{\mathbf{u}}^*_t - \alpha_3 \ddot{\mathbf{u}}^*_t;$$
$$\dot{\mathbf{u}}^*_{t+\triangle t} = \dot{\mathbf{u}}^*_t + \alpha_4 \triangle \mathbf{u}^{*i}_{t+\triangle t} - \alpha_5 \dot{\mathbf{u}}^*_t - \alpha_6 \ddot{\mathbf{u}}^*_t;$$
$$\mathbf{u}^*_{t+\triangle t} = \mathbf{u}^*_t + \triangle \mathbf{u}^{*i}_{t+\triangle t}$$

5. Compute the state of motion at teach bearing and solve for the nonlinear force at each bearing using semi-implicit Runge-kutta method.

6. Compute the resultant nonlinear force vector at the center of mass of the base $\triangle \mathbf{f}^{i+1}_{t+\triangle t}$.

7 Compute

$$Error = \frac{\left| \triangle \mathbf{f}^{i+1}_{t+\triangle t} - \triangle \mathbf{f}^i_{t+\triangle t} \right|}{Ref \cdot Max \cdot Moment}$$

Where $|\cdot|$ is the euclidean norm.

8. If Error$\geq$ tolerance, further iteration is needed, iterate starting form step B-1 and use $\triangle \mathbf{f}^{i+1}_{t+\triangle t}$ as the pseudo-force and the state of motion at time t, $\mathbf{u}^*_t$, $\dot{\mathbf{u}}^*_t$ and $\ddot{\mathbf{u}}^*_t$.

9 If Error$\leq$ tolerance, no further iteration is needed, update the nonlinear force vector: $\mathbf{f}_{t+\triangle t} = \mathbf{f}_t + \triangle \mathbf{f}^{i+1}_{t+\triangle t}$ reset time step if necessary, go to step B-1 if the time step is not reset or A-2 if the time step is reset.

10 3D-BASIS suite of computer programs

The presented formulation and solution algorithm has been implemented in—the most widely used software for analyzing base isolated structures—the class of computer programs 3D-BASIS [16,17], 3D-BASIS-M [33], 3D-BASIS-ME [34], and 3D-BASIS-TABS [35,36]. 3D-BASIS-TABS is a combination of 3D-BASIS and ETABS—a widely used building analysis software [37]. 3D-BASIS-TABS offers the advantage of modeling the superstructure using linear elastic beam,

column, and shear wall elements, while 3D-BASIS, 3D-BASIS-M, and 3D-BASIS-ME can only model the superstructure using the condensed version with 3 degrees of freedom per floor. 3D-BASIS-M and 3D-BASIS-ME offer the advantage of analyzing multiple buildings on a common isolation basemat, with the isolation system below, while only a single building on isolation system can be analyzed using 3D-BASIS and 3D-BASIS-TABS. Most recent in the series is 3D-BASIS-ME-MB, which includes the capability of model uplift [38]. 3D-BASIS class of programs are distributed through the Multidisciplinary Center for Earthquake Engineering, Buffalo, and National Information Service for Earthquake Engineering, University of California, Berkeley.

11 ETABS and SAP

The formulation in the widely used ETABS is similar to that of 3D-BASIS, but for the use of Ritz modal vectors instead of eigenvectors. Time history analysis is performed by mode superposition method. The modal equations are integrated by a method, which is exact for a linear variation of the load during the time step. The forces in the nonlinear elements are calculated at the end of each time step. The forces are treated as pseudoforces and brought on to the right hand side of the equations of motion. Iteration is then performed within the time step until convergence is achieved.

The most recent version of the widely used SAP series and ETABS series [37] are computer programs SAP and ETABS [22]. ETABS is a linear building analysis computer program and SAP is a finite element computer program. The programs have linear elastic beam, shell, plane, and solid elements. Their latest versions ETABS and SAP have discrete nonlinear elements. The nonlinear elements in the program include uniaxial and biaxial plasticity element, viscous damper element with nonlinear exponent on velocity term, gap (compression only) and hook (tension only) element, biaxial plasticity element, biaxial element for friction and/or pendulum behavior [29]. These elements allow analysis of complete three dimensional superstructure models with localized nonlinear elements such as elastomeric and friction isolators and damping devices. ETABS and SAP use a similar solution procedure to that used in 3D-BASIS. SAP and ETABS [22] are proprietary computer programs of Computers and Structures Inc., Berkeley, CA.

12 Key Innovations

The acronym 3D-BASIS stands for **3D-BAS**e **I**solated **S**tructures, coined by the author in 1989. Several key innovations in formulation and computational

techniques, needed in the development of 3D-BASIS, have been summarized in this chapter. Briefly,

1. New Nonlinear/Inelastic Analytical Models for Elastomeric Bearings, Sliding Bearings, Three Dimensional Sliding and Elastomeric Base Isolated Structures
2. Formulation of the Pseudo-force Solution Algorithm, Semi-Implicit Algorithm, and proof of Convergence using Closed Form Solutions [15]
3. Due to highly nonlinear biaxial interaction for sliding isolation bearings, the differential equations become very stiff and even Gear's predictor-corrector method for stiff differential equation fails
4. Formulated a new stable semi implicit integration method based on Rosenbrock's [31] method
5. Integration Coefficients 0.78886751 and -1.1547005 were derived originally by Nagarajaiah [15] to maintain a fourth order truncation error
6. Verification using extensive shake table test results.

13 3D-BASIS used for Analysis of Important Base Isolation Projects Around the World:

3D-BASIS for Nonlinear Dynamic Analysis of Base Isolated Structures has been cited in several important code related documents [FEMA 273/274 [39], ATC 33, NEHRP, NIST]. "The most widely used computer program for analyzing base isolated structures today is the 3D-BASIS suite of programs..." is a direct quote from the book on "Earthquake Resistant Design with Rubber" by Professor James M. Kelly, 1997 [2]—see page 234.

3D-BASIS has been used for analysis and design of numerous projects around the world; the most important of which are listed below.

- U. S. Court of Appeals, San Francisco, CA, 1990-1991
- LNG Tanks, Greece, 1994
- San Francisco International Airport, CA, 1996
- ATATURK International Airport in Istanbul, Turkey, 2000
- Statue of Hermes, Museum at Olympia, Greece, 2004
- Mills Peninsula Hospital, Burlingame, CA, 2005-Currently Complete
- Washington Hospital, Fremont, CA, 2005-Currently Complete
- Stanford University Hospital, CA, 2008 – Currently complete
- Lunskoye and Piltun Offshore Oil Platforms, Sakhalin, Russia, 2008 – Currently Complete
- San Francisco General Hospital, CA, 2011 – under construction

- Arkundagi Offshore Oil Platform, Sakhalin, Russia, 2013 – Under Construction

12 Concluding remarks

3D-BASIS release was significant milestone in nonlinear dynamic analysis of three-dimensional base isolated structures, particularly in solving the highly nonlinear bidirectional stick-slip hysteretic response of a collection of sliding isolation bearings and the resulting response of the superstructure. In this chapter techniques used in the nonlinear dynamic analysis of base isolated structures in 3D-BASIS have been presented. These techniques developed by the author and other researchers have been implemented in the latest NEHRP Guidelines / Commentary for the Seismic Rehabilitation of Buildings (Ballot Version) FEMA 273/274 [39]. The presented nonlinear dynamic techniques and computer programs have been widely used in the analysis and design of many new and retrofit base isolation projects around the United States and also around the world. In summary,

- 3D-BASIS has had a unique impact on nonlinear dynamic analysis of base isolated structures around the world
- SAP uses the similar formulation as in 3D-BASIS; for more detail refer to Wilson et al. [28] and SAP-ETABS [22].
- The latest version of 3D-BASIS—3D-BASIS-MB-ME—Includes Triple Pendulum Model, uplift and new response prediction and display features.

Results from OpenSees [40] and SAP-ETABS [22], which are widely used currently in earthquake engineering simulation, are verified using 3D-BASIS suite of programs by many researchers and practitioners [41]. In addition now that Structural Health Monitoring is being adopted steadily more real measured data will become available to validate and verify any future developments [30,42].

Acknowledgments 3D-BASIS suite of computer programs would not have been possible without the vision of Professor Andrei Reinhorn. 3D-BASIS suite of computer programs has been realized by the sustained efforts of the author, Professor Andrei Reinhorn, and his collaborators at University at Buffalo.

References

[1] Buckle, I. G., and Mayes, R. L. (1990) "Seismic Isolation: history, application, and performance—A world overview," *Earthquake Spectra*, 6(2), 161-202.
[2] Kelly, J.M. (1997) *Earthquake-Resistant Design with Rubber,* 2nd Ed., Springer, New York.
[3] Skinner, R.I., Johnson, H., McVerry, H. (1993) *Introduction to Seismic Isolation,* J. Wiley, NY.

[4] Soong, T.T. and Constantinou, M.C., (1994) *Passive and Active Structural Vibration Control in Civil Engineering,* Springer-Verlag, New York.
[5] Constantinou, M.C., Whittaker, A. S., Kalpakidis, Y., Fenz, D. M., and Warn, G. P. (2007). "Performance of seismic isolation hardware under service and seismic loading," Technical Report MCEER-07-0012.
[6] Tsopelas, P., Nagarajaiah, S., Constantinou, M. C., and Reinhorn, A. M., (1994) "Nonlinear dynamic analysis of multiple building base isolated structures," Journal of Computers and Structures, Vol. 50, No. 1, 47-57.
[7] Kikuchi, M., and Aiken, I.D. (1997) "An analytical hysteresis model for elastomeric seismic isolation bearings," *Earthquake Eng. Struct. Dyn.,* Vol. 26, No.2, 214-231.
[8] Constantinou, M.C., Mokha, A., and Reinhorn, A.M. (1990). "Teflon bearings in base isolation II: Modeling*," J. Struct. Eng*., ASCE, 16(4), 455-474.
[9] Fenz DM, Constantinou MC. (2008a) "Spherical sliding isolation bearings with adaptive behavior: Theory," Earthquake Engineering and Structural Dynamics 2008; 37(2):163-183.
[10] Fenz DM, Constantinou MC. (2008b) Modeling triple friction pendulum bearings for response-history analysis. Earthquake Spectra; 24(4):1011–1028.
[11] Morgan TA, Mahin SA. (2011) "The use of innovative base isolation systems to achieve complex seismic performance objectives," PEER-Center-Report 2011/06, UC Berkeley.
[12] Ray, T. and Reinhorn, A. (2012) "Enhanced Smooth Hysteretic Model with Degrading Properties." J. Struct. Eng., 10.1061/(ASCE)ST.1943-541X.0000798 (Dec. 29, 2012).
[13] Dao ND, Ryan KL, Sato E, Sasaki T. (2013) "Predicting the displacement of triple pendulum™ bearings in a full-scale shaking experiment using a three-dimensional element," Earthquake Engineering and Structural Dynamics, DOI: 10.1002/eqe.2293.
[14] Constantinou, M.C., and Symans, M. D. (1993) "Experimental study of seismic response of buildings with supplemental fluid dampers," *J. Struct. Design of Tall Buildings,* Vol. 2, 93-132.
[15] Nagarajaiah, S. (1990), "Nonlinear Dynamic Analysis of Three Dimensional Base Isolated Structures," Ph.D. Dissertation, University at Buffalo.
[16] Nagarajaiah, S., Reinhorn, A. M. and Constantinou, M. C. (1991a) "3D-BASIS Nonlinear Dynamic Analysis of Three Dimensional Base Isolated Structures: Part II," *Report No. 91-0005*, National Ctr. for Earthquake Eng. Res., University of Buffalo, NY.
[17] Nagarajaiah, S., Reinhorn, A. M. and Constantinou, M. C. (1991b) "Nonlinear Dynamic Analysis of Three Dimensional Base Isolated Structures," *J. Struct. Eng.*, ASCE, Vol.117, No.7, 2035-2054.
[18] Bouc, R. (1967) Forced Vibration of Mechanical Systems with Hysteresis. Proceedings 4th Conference on Nonlinear Oscillations, Prague. See also "Mathematical Model for Hysteresis." Report to Centre de Recherches Phy-siques, Marseille, France, pp.16-25.
[19] Wen, Y. K. (1976) "Method of random vibration of hysteretic systems," *J. Struct. Eng.*, ASCE, Vol.117, No.7, 2035-2054.
[20] Park, Y. J., Wen, Y. K., and Ang, A.H.S. (1986) "Random vibration of hysteretic systems under bidirectional ground motions," *Earthquake Eng. Struct. Dyn.*, 11(6), 749-770.
[21] Mokha, A., Constantinou, M C., and Reinhorn, A.M. (1993) "Verification of Friction Model of Teflon bearings under triaxial Load," *J. Struct. Eng.*, ASCE, Vol.119, No.1, 240-261.
[22] SAP-ETABS, (2014) *Structural analysis and Design Software*, Computers and Structures Inc., CA.
[23] Buckle I.G., and Kelly, J. (1986) "Properties of slender elastomeric isolation bearings during shake table studies of a large scale model bridge deck," *Joint Sealing and Bearing Systems*, ACI, Vol.1, 247-269.
[24] Nagarajaiah, S. (1995). "Seismic response of multistory sliding isolated structures with uplift," *Proc. Structures Congress '95*, ASCE, Boston, Massachusetts, 1044-1047.
[25] Koh, C. G., and Kelly, J. M. (1986) "Effects of axial load on elastomeric bearings," *Report No. UCB/EERC-86/12*, Earthquake Eng. Res. Ctr., University of California, Berkeley, CA.
[26] Nagarajaiah, S., and Ferrell, K. (1999) "Stability of elastomeric seismic isolation bearings," Journal of Structural Engineering, ASCE, Vol. 125, No. 9, 946-954.

[27] Nagarajaiah, S., Reinhorn, A. M., and Constantinou, M. C., (1992) "Experimental study of sliding isolated structures with uplift restraint," Journal of Structural Engineering, ASCE, Vol. 118, No. 6, 1666-1682.

[28] Wilson, E.L. (1993) "An efficient computational method for the base isolation and energy dissipation analysis of structural systems," *Proc. Seminar on Seismic Isolation, Passive Energy Dissipation*, ATC 17-1, 365-376

[29] Scheller, J. and Constantinou, M. C. (1998) " Response History Analysis of Structures with Seismic Isolation and Energy Dissipation Systems: Verification Examples for Program SAP2000," *Technical Report No. 99-0002*, Multidisciplinary Ctr. for Earthquake Eng. Res., Univ. of Buffalo, NY.

[30] Nagarajaiah, S., and Sun, X., (2001) "Base Isolated FCC building: Impact Response in Northridge Earthquake," Journal of Structural Engineering, ASCE, Vol. 127, No. 9, 1063-1074.

[31] Rosenbrock, H. H. (1964) "Some general implicit processes for numerical solution of differential equations," *Computing Journal*, 18(1), 50-64.

[32] Reinhorn, A. (1994), Personal Communication with Professor Reinhorn.

[33] Tsopelas, P., Nagarajaiah, S., Constantinou, M. C. and Reinhorn, A. M. (1991) "3D-BASIS-M: Nonlinear Dynamic Analysis of Multiple Building Base Isolated Structures," *Report No. 91-0014*, National Ctr. for Earthquake Eng. Res., Univ. of Buffalo, NY.

[34] Tsopelas, P., Constantinou, M. C. and Reinhorn, A. M. (1994) "3D-BASIS-ME: Nonlinear Dynamic Analysis of Seismically Isolated Single and Multiple Structures," *Report No. 94-0010*, National Ctr. for Earthquake Eng. Res., Univ. of Buffalo, NY.

[35] Nagarajaiah, S., Li, C., Reinhorn, A.M., and Constantinou, M.C. (1993) "3D-BASIS-TABS Computer Program for Nonlinear Dynamic Analysis of Three Dimensional Base Isolated Structures," *Report NCEER-93-0011*, National Ctr. for Earthquake Eng. Res., Buffalo, NY.

[36] Reinhorn, A. M., Nagarajaiah, S., Constantinou, M.C., Tsopelas, P., and Li, R. (1994) "3D-BASIS-TABS: V2.0 Computer Program for Nonlinear Dynamic Analysis of 3D Base Isolated Structures," *Technical Report No. 94-0018*, National Ctr.for Earthquake Eng. Res., Univ. of Buffalo, NY.

[37] Wilson, E.L., Hollings, J.P., and Dovey, H.H. (1975) "ETABS – Three dimensional analysis of building systems." *Report No. UCB/EERC-75/13*, Earthquake Eng. Res. Center, Univ. of California, Berkeley, CA.

[38] Tsopelas, P., Roussis, P.C., Constantinou, M.C., Buchanan, R., and Reinhorn, M. (2005) "3D-BASIS-ME-MB: Computer Program for Nonlinear Dynamic Analysis of Seismically Isolated Structures" *Technical Report No. MCEER-05-0009*, Multidisciplinary Ctr. for Earthquake Eng. Res., Univ. of Buffalo, NY.

[39] FEMA 273/274 (1997) *NEHRP Guidelines / Commentary for the Seismic Rehabilitation of Buildings ,* Federal Emergency Management Agency.

[40] OpenSees (2014) Open System for Earthquake Engineering Simulation, An open-source program available at http://opensees.berkeley.edu.

[41] Sarkisian, M. and Lee, P. (mark.sarkisian@som.com, peter.lee@som.com), (2011), Personal communication (S.M.-Engineering Director and L.P., Associate Director), Skidmore, Owings & Merrill, San Francisco, Mar 7, 2011.

[42] Nagarajaiah, S., and Sun, X., (2000) "Response of base isolated USC hospital building in Northridge Earthquake," Journal of Structural Engineering, ASCE, Vol. 126, No. 10, 1177-1186.